







# Microstructure and Mechanical Properties of Composites Obtained by Spark Plasma Sintering of Al–Fe<sub>66</sub>Cr<sub>10</sub>Nb<sub>5</sub>B<sub>19</sub> Metallic Glass Powder Mixtures

Dina V. Dudina <sup>1,2,3,\*</sup> , Boris B. Bokhonov <sup>3</sup> , Igor S. Batraev <sup>1</sup> , Vyacheslav I. Kvashnin <sup>1,2</sup>, Mikhail A. Legan <sup>1,2</sup> , Aleksey N. Novoselov <sup>1</sup>, Alexander G. Anisimov <sup>1</sup>, Maksim A. Esikov <sup>1,2</sup> , Arina V. Ukhina <sup>3</sup>, Alexander A. Matvienko <sup>3</sup>, Konstantinos Georgarakis <sup>4</sup>, Guilherme Yuuki Koga <sup>5</sup> and Alberto Moreira Jorge, Jr. <sup>5,6,7</sup> 

- <sup>1</sup> Lavrentyev Institute of Hydrodynamics SB RAS, Lavrentyev Ave. 15, 630090 Novosibirsk, Russia; ibatraev@gmail.com (I.S.B.); slava.kvashnin@mail.ru (V.I.K.); legan@ngs.ru (M.A.L.); aleksey.novoselov@gmail.com (A.N.N.); anis@hydro.nsc.ru (A.G.A.); esmax@ya.ru (M.A.E.)
- <sup>2</sup> Novosibirsk State Technical University, K. Marx Ave. 20, 630073 Novosibirsk, Russia
- <sup>3</sup> Institute of Solid State Chemistry and Mechanochemistry SB RAS, Kutateladze Str. 18, 630128 Novosibirsk, Russia; bokhonov@solid.nsc.ru (B.B.B.); auhina181@gmail.com (A.V.U.); matvienko67@gmail.com (A.A.M.)
- <sup>4</sup> School of Aerospace, Transport and Manufacturing, Cranfield University, Cranfield MK43 0AL, UK; K.Georgarakis@cranfield.ac.uk
- <sup>5</sup> Department of Materials Science and Engineering, Federal University of São Carlos, Via Washington Luiz, km 235, São Carlos 13565-905, SP, Brazil; guilherme.koga@gmail.com (G.Y.K.); moreira@ufscar.br or alberto.moreira-jorge-junior@grenoble-inp.fr (A.M.J.J.)
- <sup>6</sup> The Laboratory of Electrochemistry and Physical-Chemistry of Materials and Interfaces (LEPMI), Université Grenoble Alpes, Université Savoie Mont Blanc, CNRS, Grenoble IN, 38000 Grenoble, France
- <sup>7</sup> Science et Ingénierie des Matériaux et Procédés (SMiAP), Université Grenoble Alpes, CNRS, Grenoble IN, 38000 Grenoble, France
- \* Correspondence: dina1807@gmail.com



**Citation:** Dudina, D.V.; Bokhonov, B.B.; Batraev, I.S.; Kvashnin, V.I.; Legan, M.A.; Novoselov, A.N.; Anisimov, A.G.; Esikov, M.A.; Ukhina, A.V.; Matvienko, A.A.; et al. Microstructure and Mechanical Properties of Composites Obtained by Spark Plasma Sintering of Al–Fe<sub>66</sub>Cr<sub>10</sub>Nb<sub>5</sub>B<sub>19</sub> Metallic Glass Powder Mixtures. *Metals* **2021**, *11*, 1457. <https://doi.org/10.3390/met11091457>

Academic Editors: Qingping Cao, Golden Kumar and Jordi Sort Viñas

Received: 26 June 2021

Accepted: 10 September 2021

Published: 15 September 2021

**Publisher's Note:** MDPI stays neutral with regard to jurisdictional claims in published maps and institutional affiliations.



**Copyright:** © 2021 by the authors. Licensee MDPI, Basel, Switzerland. This article is an open access article distributed under the terms and conditions of the Creative Commons Attribution (CC BY) license (<https://creativecommons.org/licenses/by/4.0/>).

**Abstract:** At present, metallic glasses are evaluated as alternative reinforcements for aluminum matrix composites. These composites are produced by powder metallurgy via consolidation of metallic glass-aluminum powder mixtures. In most studies, the goal has been to preserve the glassy state of the reinforcement during consolidation. However, it is also of interest to track the structure evolution of these composites when partial interaction between the matrix and the metallic glass is allowed during sintering of the mixtures. The present work was aimed to study the microstructure and mechanical properties of composites obtained by spark plasma sintering (SPS) of Al-20 vol.% Fe<sub>66</sub>Cr<sub>10</sub>Nb<sub>5</sub>B<sub>19</sub> metallic glass mixtures and compare the materials, in which no significant interaction between the matrix and the Fe-based alloy occurred, with those featuring reaction product layers of different thicknesses. Composite materials were consolidated by SPS at 540 and 570 °C. The microstructure and mechanical properties of composites obtained by SPS and SPS followed by forging, composites with layers of interfacial reaction products of different thicknesses, and metallic glass-free sintered aluminum were comparatively analyzed to conclude on the influence of the microstructural features of the composites on their strength.

**Keywords:** metallic glass; metal matrix composite; interfacial reaction; reinforcement; mechanical properties

## 1. Introduction

A traditional metal matrix composite is a metal matrix in which ceramic particles or fibers are distributed [1]. A large difference between the coefficients of thermal expansion of the phases and low wettability at the interface are problems common to this class of materials. Recent years have seen active research in the area of aluminum matrix composites directed at evaluating the suitability of alternative (non-ceramics) reinforcements. In novel

composites, particles of intermetallics [2,3], quasicrystals [4], high-entropy alloys [5,6], or metallic glasses [7–14] are used as the reinforcing elements. These composites are usually produced by powder metallurgy via consolidation of mixtures of the matrix metal and metallic alloy powders.

Two types of amorphous alloy-containing composites can be designed: with a crystalline metal matrix or an amorphous alloy matrix. If the matrix phase is glassy, the addition of crystalline particles causes a decrease in strength and an increase in ductility [15]. If the matrix is crystalline, the addition of glassy particles causes an increase in strength. The advantages of metallic glass particles as a reinforcing phase are the high strength of metallic glass and its better wettability by the matrix metal than the wettability of ceramic particles by the same metal. Furthermore, if consolidation of the powder mixture occurs within the supercooled liquid region of the metallic glass, the latter acts as a binder, efficiently filling the pores [10,11].

In most studies dealing with metallic glass-aluminum mixtures, the goal has been to preserve the glassy state of the reinforcement during the formation of the bulk material. Composites have been obtained, in which the layers forming at the metal matrix/metallic glass interface possess very small thicknesses (in the nanometer range) [12,14]. When a particle introduced into a matrix starts chemically interacting with it, a core-shell structure forms upon partial consumption of the particle material. Core-shell particles are also attracting interest as possible reinforcements with a unique mechanical behavior [16]. The formation of particles of core-shell structure in metallic glass particle-reinforced aluminum matrix composites was given particular attention in ref. [17]. The composites were obtained by spark plasma sintering (SPS) followed by hot rolling. In those composites,  $\text{Fe}_{50}\text{Cr}_{25}\text{Mo}_9\text{C}_{13}\text{B}_3$  metallic glass particles were embedded in aluminum and partially reacted with it. The reinforcement content was varied, while the processing conditions were the same for the studied series of composites. The authors suggested that a certain degree of crystallization on the surface of metallic glass particles may lead to stronger interfacial bonding.

When the quantity of the  $\text{FeAl}_3$  intermetallic, the product of the interaction of the Al matrix and the Fe-based metallic glass, is limited and its distribution is discontinuous, the ductility of the composites will not be affected. It should be noted that  $\text{FeAl}_3$  itself can serve as a reinforcing phase stable in an Al matrix. For example, an Al- $\text{FeAl}_3$  composite containing 16 vol.% of  $\text{FeAl}_3$  showed an increased yield strength in compression (190 MPa) [2].

Fe-based metallic glasses are known for their high hardness and corrosion resistance [18].  $\text{Fe}_{66}\text{Cr}_{10}\text{Nb}_5\text{B}_{19}$  amorphous alloy powders are easily obtained by gas atomization using commercial alloys as raw materials [13]. This makes  $\text{Fe}_{66}\text{Cr}_{10}\text{Nb}_5\text{B}_{19}$  alloy powders with a glassy structure attractive for the reinforcing purposes. In the Fe-Al system, interdiffusion of the metals occurs during alloying [19,20]. So, in Al- $\text{Fe}_{66}\text{Cr}_{10}\text{Nb}_5\text{B}_{19}$  composites, bonding at the interface may be possible through the formation of transition zones caused by diffusion of iron along with other components of the metallic glass into aluminum and aluminum into the metallic glass.

Our previous study reported the hardness of composites obtained by SPS of Al- $\text{Fe}_{66}\text{Cr}_{10}\text{Nb}_5\text{B}_{19}$  mixtures and the microhardness of separate phases [13]. The present work was aimed to study the microstructural features and mechanical properties of composites obtained by SPS of Al-20 vol.%  $\text{Fe}_{66}\text{Cr}_{10}\text{Nb}_5\text{B}_{19}$  mixtures and compare composites, in which no significant interaction between the matrix and the Fe-based alloy occurred, with those featuring reaction product layers of different thicknesses.

## 2. Materials and Methods

In the present study, gas-atomized powders of  $\text{Fe}_{66}\text{Cr}_{10}\text{Nb}_5\text{B}_{19}$ , <45  $\mu\text{m}$  fraction [13] and aluminum were used. The Al powder had a purity of 99.9% (PAD-6, average particle size 6  $\mu\text{m}$ , “VALKOM-PM”, Volgograd, Russia). Al- $\text{Fe}_{66}\text{Cr}_{10}\text{Nb}_5\text{B}_{19}$  mixtures containing 20 vol.% of the glassy alloy were prepared by mixing in a custom-made horizontal low-energy device (a plastic container with steel balls).

Sintering of the powders was carried out using a SPS Labox 1575 apparatus (SINTER LAND Inc., Nagaoka, Japan) in forevacuum at a uniaxial pressure of 40 MPa. SPS was selected for its ability of rapid heating and consolidation of powders containing metastable phases [21]. The tooling consisted of a graphite die of 20 mm inner diameter and graphite punches. Al-Fe<sub>66</sub>Cr<sub>10</sub>Nb<sub>5</sub>B<sub>19</sub> mixtures were subjected to SPS at 540 and 570 °C. The heating rate was 50 °C·min<sup>-1</sup>. The holding time at the maximum temperature was 3 min. Samples were also obtained without the soaking stage at the maximum temperature. The aluminum powder was sintered by heating up to 540 °C without soaking at this temperature to produce a reference material. For forging, a 10 mm diameter Al-Fe<sub>66</sub>Cr<sub>10</sub>Nb<sub>5</sub>B<sub>19</sub> cylinder was first sintered using a 10 mm graphite die. The cylinder had a height of 12 mm. It was further processed in a 20 mm diameter die: the applied force was increased from 3 to 10 kN in a stepwise manner, while the temperature was increased up to 450 °C. The holding time at this temperature was 3 min, after which the current was switched off. The final load of 10 kN was maintained during the cooling stage. The total forging operation time was 30 min. The forged sample has a diameter of 20 mm.

The morphology of the powders and microstructure of the sintered samples was studied by scanning electron microscopy (SEM) using a TM-1000 Tabletop microscope (Hitachi, Tokyo, Japan), a Carl Zeiss EVO 50 XVP microscope (Oberkochen, Germany), and a S-3400N (Hitachi, Tokyo, Japan) microscope. Energy-dispersive spectroscopy (EDS) was conducted using a NORAN Spectral System 7 (Thermo Fisher Scientific Inc., Waltham, MA, USA). X-ray diffraction (XRD) patterns of the samples were recorded by a D8 ADVANCE diffractometer (Bruker AXS, Karlsruhe, Germany) with Cu K $\alpha$  radiation.

The porosity of the sintered materials was determined from the cross-sectional images of the samples using ImageJ software (<https://imagej.nih.gov>). The volume contents of the matrix in the composites sintered at 540 and 570 °C for 3 min were reduced relative to that in the initial powder mixture. The matrix contents in those composites were also determined using ImageJ software. For that purpose, 15 images of the cross-sections of the composites recorded at  $\times 500$  magnification were analyzed.

Samples for compression tests were cut from the sintered disks to  $3 \times 3 \times 6$  mm<sup>3</sup> dimensions. The compression tests were conducted using a Zwick/Roell Z100 device (Ulm, Germany) at a crosshead speed of 0.1 mm·min<sup>-1</sup>. The compression direction of the sample was normal to the pressing direction during SPS. The average values of the offset yield strength and ultimate strength of the composites were determined from three measurements.

### 3. Results and Discussion

Figure 1 shows the morphology of Fe<sub>66</sub>Cr<sub>10</sub>Nb<sub>5</sub>B<sub>19</sub> and aluminum powders and the XRD pattern of the Fe<sub>66</sub>Cr<sub>10</sub>Nb<sub>5</sub>B<sub>19</sub> powder. The particles of both powders possess spherical shape. The XRD pattern of the Fe<sub>66</sub>Cr<sub>10</sub>Nb<sub>5</sub>B<sub>19</sub> powder demonstrates a halo between 40° and 50° (2 $\theta$ ), indicating the presence of an amorphous phase. Indeed, the Fe<sub>66</sub>Cr<sub>10</sub>Nb<sub>5</sub>B<sub>19</sub> powder is predominantly amorphous: the concentration of the crystalline phase (body-centered cubic iron) is ~5 wt.%, as determined in our previous work [22]. The glass transition temperature and crystallization temperature of the glassy phase in the Fe<sub>66</sub>Cr<sub>10</sub>Nb<sub>5</sub>B<sub>19</sub> alloy is 521 and 573 °C, respectively [13].

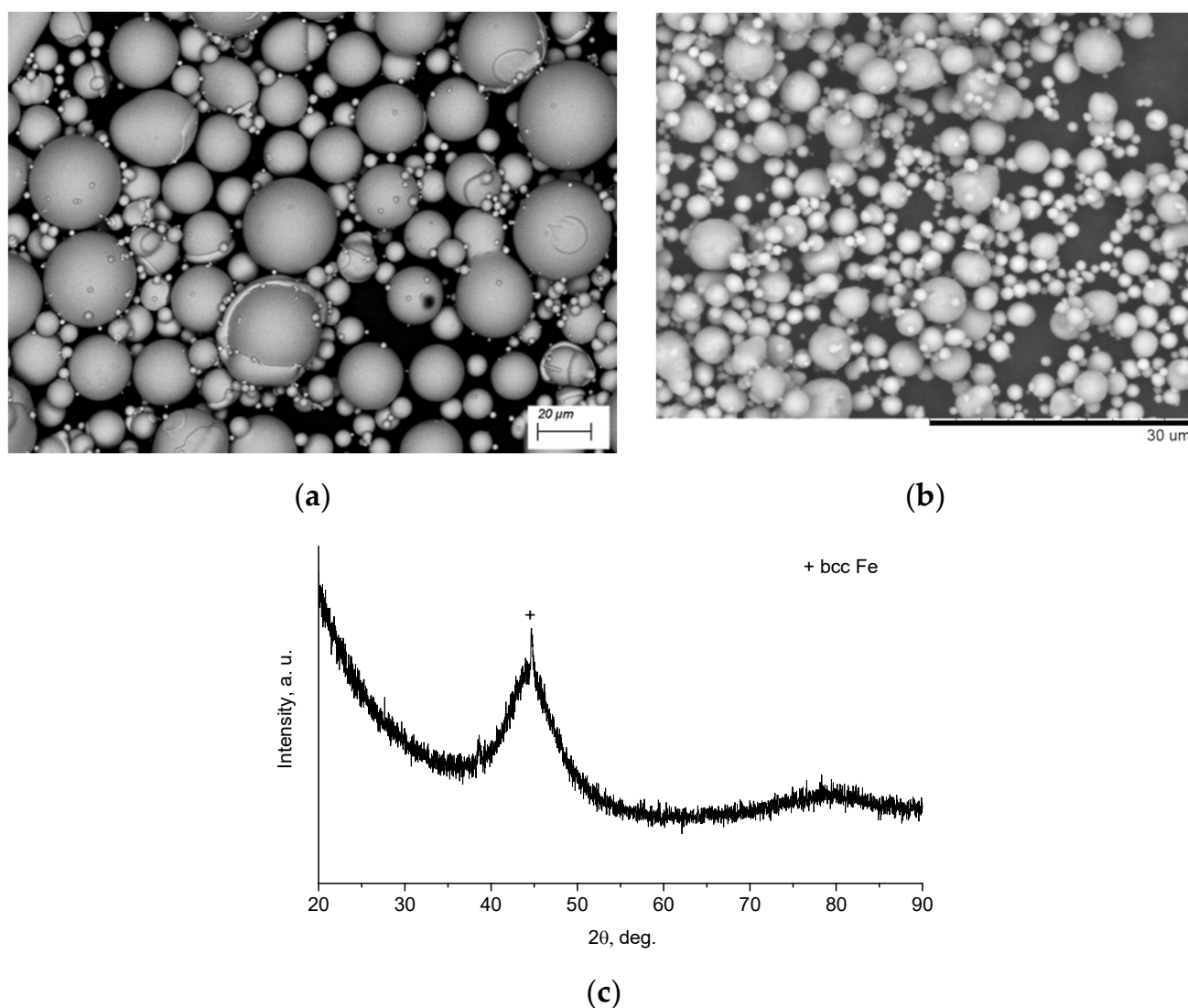


**Figure 1.** (a) Scanning electron microscopy (SEM) image of the  $\text{Fe}_{66}\text{Cr}_{10}\text{Nb}_5\text{B}_{19}$  metallic glass powder, back-scattered electron (BSE) image, (b) SEM image of the aluminum powder, back-scattered electron image, (c) X-ray diffraction (XRD) pattern of the  $\text{Fe}_{66}\text{Cr}_{10}\text{Nb}_5\text{B}_{19}$  metallic glass powder. The minor phase in the alloy is body-centered cubic iron (bcc-Fe).

The composites were obtained by sintering at two temperatures (540 and 570 °C) to produce reaction product layers of different thicknesses. The forging operation was attempted to break the oxide film present on the particle surfaces and improve the inter-particle bonding.

Figure 2 shows the XRD patterns of the sintered composites. As seen in Figure 2a, reflections of aluminum are present in the patterns of composites obtained by SPS at 540 °C without holding and SPS followed by forging. No reflections of the reaction products between the metallic glass and aluminum are observed. Enlarged portions of the XRD patterns (35–50°, 2 $\theta$ ) are shown in Figure 2b,c. A diffraction halo between 40° and 50° overlapping with a reflection of aluminum indicates the presence of an amorphous phase in the sintered material. Therefore, in these composites, the glass phase of the Fe-based alloy was preserved after consolidation.

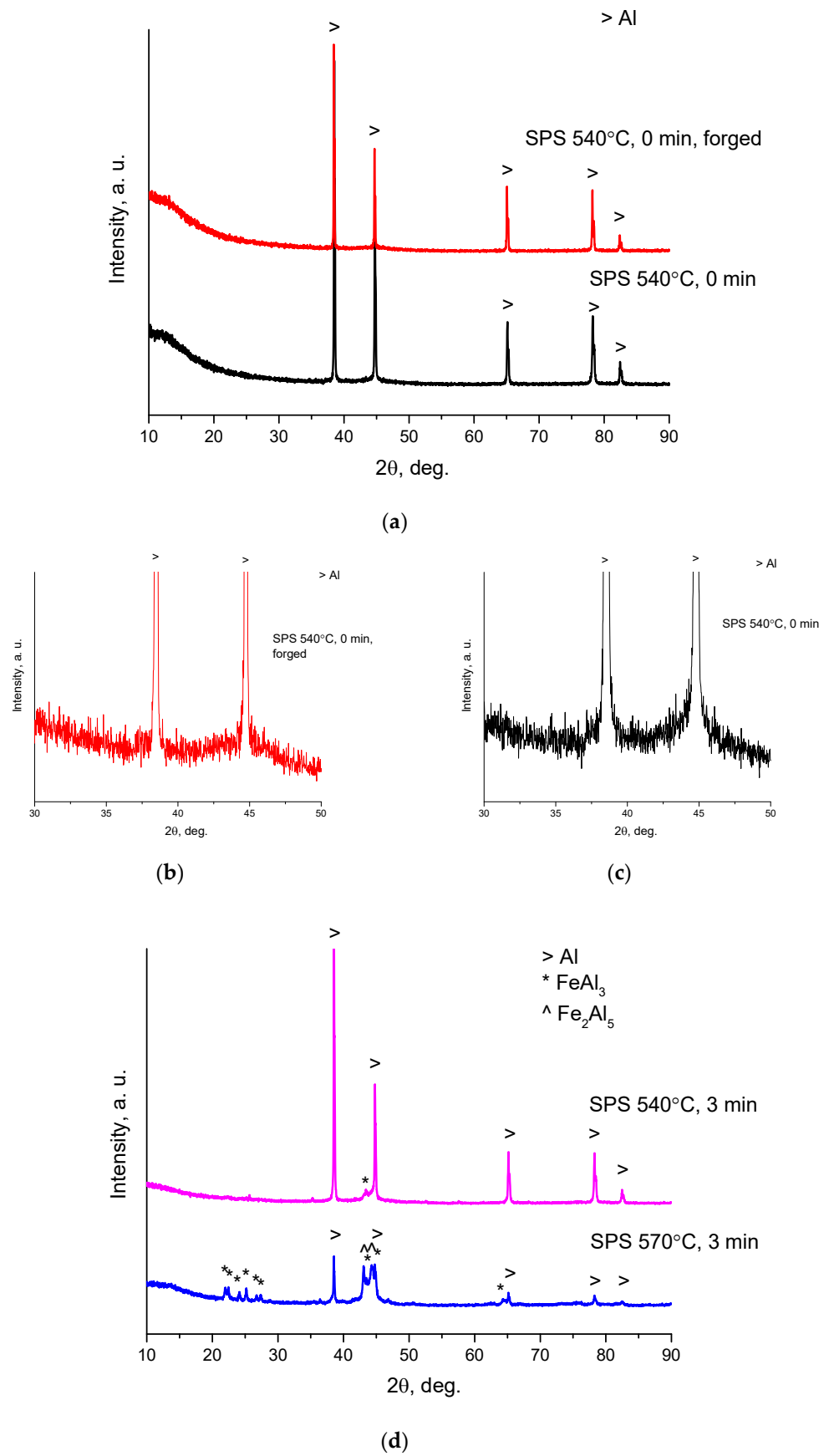
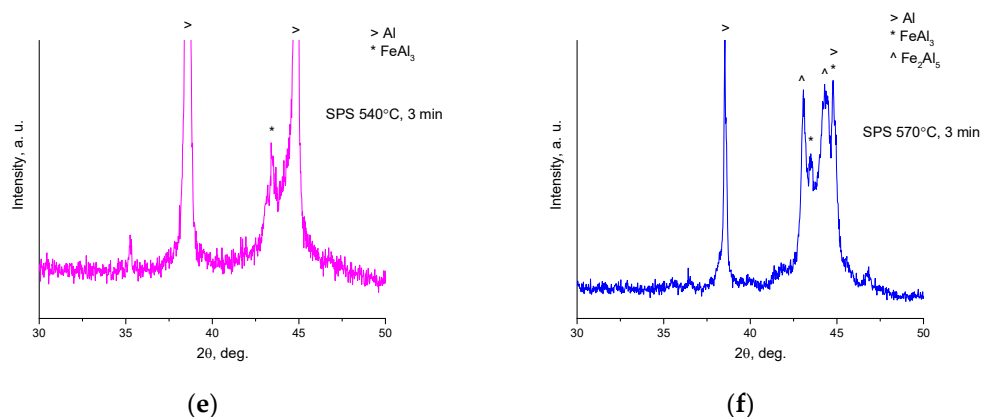


Figure 2. Cont.



**Figure 2.** XRD patterns of composites obtained from Al-20 vol.% Fe<sub>66</sub>Cr<sub>10</sub>Nb<sub>5</sub>B<sub>19</sub> mixtures: (a) spark plasma sintering (SPS) at 540 °C, no holding, and SPS at 540 °C, no holding/forging at 450 °C; (b,c) enlarged portions (30–50°) of the XRD patterns of samples shown in (a); (d) SPS at 540 °C, 3 min, and SPS at 570 °C, 3 min; (e,f) enlarged portions (30–50°) of the XRD patterns of samples shown in (d).

In the pattern of the sample held for 3 min at 540 °C, a broad reflection belonging to the FeAl<sub>3</sub> phase appears (Figure 2d). Reflections of FeAl<sub>3</sub> are much more pronounced in the pattern of the sample sintered at 570 °C for 3 min. Along with reflections of FeAl<sub>3</sub>, those of Fe<sub>2</sub>Al<sub>5</sub> are detected. In the enlarged portions of the XRD patterns (Figure 2e,f), a diffraction halo can also be distinguished (overlapping with reflections of the crystalline phases), pointing to the presence of an amorphous phase in the sintered composites, possibly in reduced concentrations relative to composites sintered at 540 °C.

The microstructure of the material sintered at 540 °C without holding and that obtained by SPS/forging are similar (Figure 3a,b). No reaction layer is seen at the interface between the matrix and the reinforcement. The spherical particles of the Fe-based alloy do not show any grain boundary structure, which agrees with results of the XRD analysis of these samples. Holding of the sample at 540 °C for 3 min resulted in the growth of the reaction product layer around the spherical particles of the alloy (Figure 3c and enlarged image in Figure 4a). After sintering at 570 °C for 3 min, the layer grew even further (Figure 3d and enlarged image in Figure 4b).

The EDS profiles show that, in the composite sintered at 540 °C without holding, the concentrations of Al, Fe, and Cr change rapidly with distance when the particle/matrix boundary is crossed (Figure 5). The product layer formed after sintering at 540 °C for 3 min has a gradient structure (Figure 6). If extrapolated, the Fe and Cr downhill lines corresponding to the reaction product layer intersect the x-axis almost at the same point, so the ratio of the Fe and Cr concentrations in this layer remains constant. Guan et al. [17] used transmission electron microscopy to study the structure of the interfacial layers in composites consolidated from Al-Fe<sub>50</sub>Cr<sub>25</sub>Mo<sub>9</sub>C<sub>13</sub>B<sub>3</sub> mixtures. Three areas were detected: amorphous regions containing diffused Al atoms, crystallized regions containing Al atoms, and FeAl<sub>3</sub> intermetallic.

The formation of pores in the metallic systems during heat treatment due to the Kirkendall effect is a known phenomenon [23–25]. When an Al matrix composite with embedded Cu particles was heat-treated, pores formed in the Cu particles due to the Kirkendall effect [23]. When aluminum is surrounded by iron, pores form in the locations of aluminum particles [24,25]. Studying the Kirkendall effect in Al-Fe<sub>66</sub>Cr<sub>10</sub>Nb<sub>5</sub>B<sub>19</sub> requires carrying out model experiments under conditions that are not necessarily optimal for making composites with attractive mechanical properties. Therefore, this issue was not addressed in the present work and will be dealt with in a separate investigation.



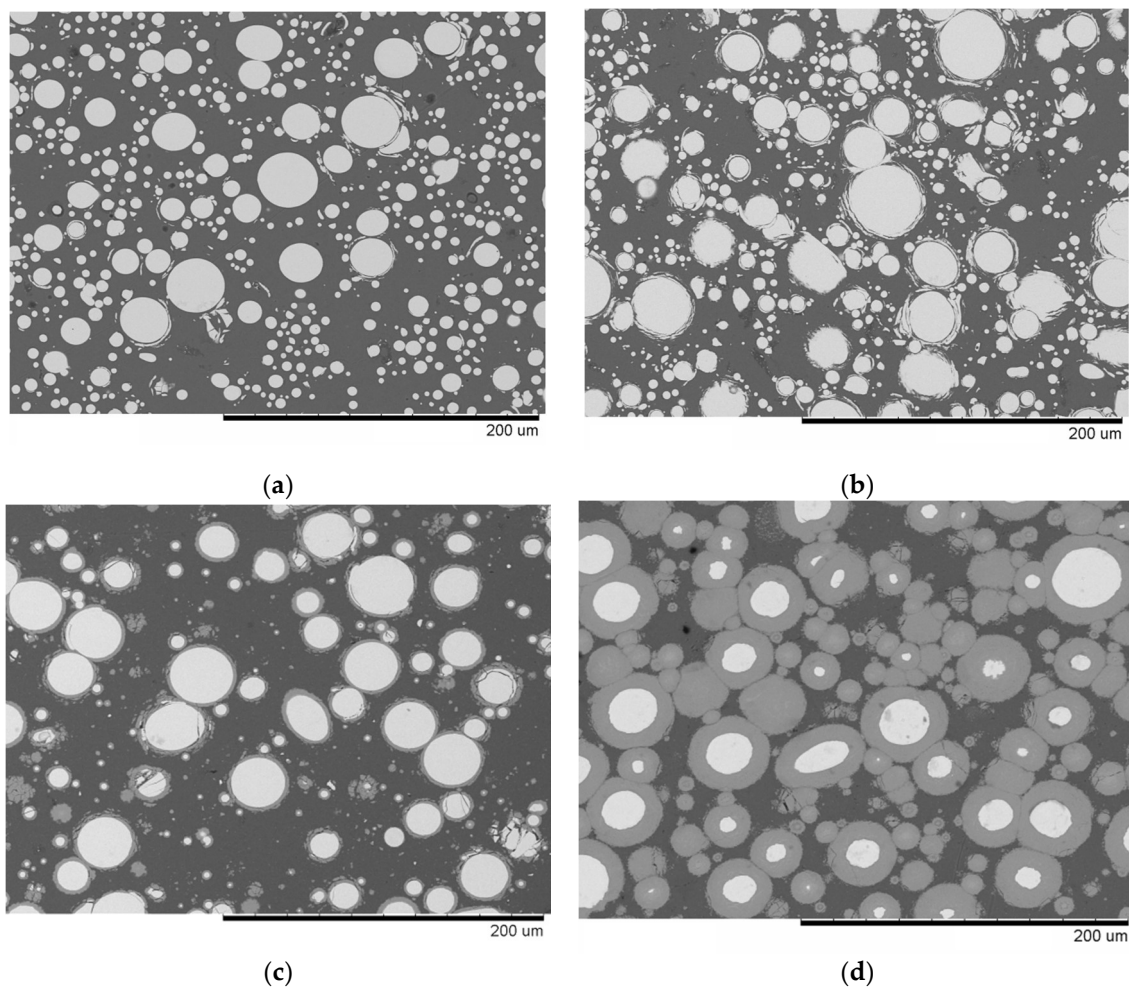


**Figure 3.** Microstructure of composites obtained from Al-20 vol.%  $\text{Fe}_{66}\text{Cr}_{10}\text{Nb}_5\text{B}_{19}$  mixtures: (a) SPS at 540 °C, no holding, (b) SPS at 540 °C, no holding, and forging, (c) SPS at 540 °C, 3 min, (d) SPS at 570 °C, 3 min. BSE images.

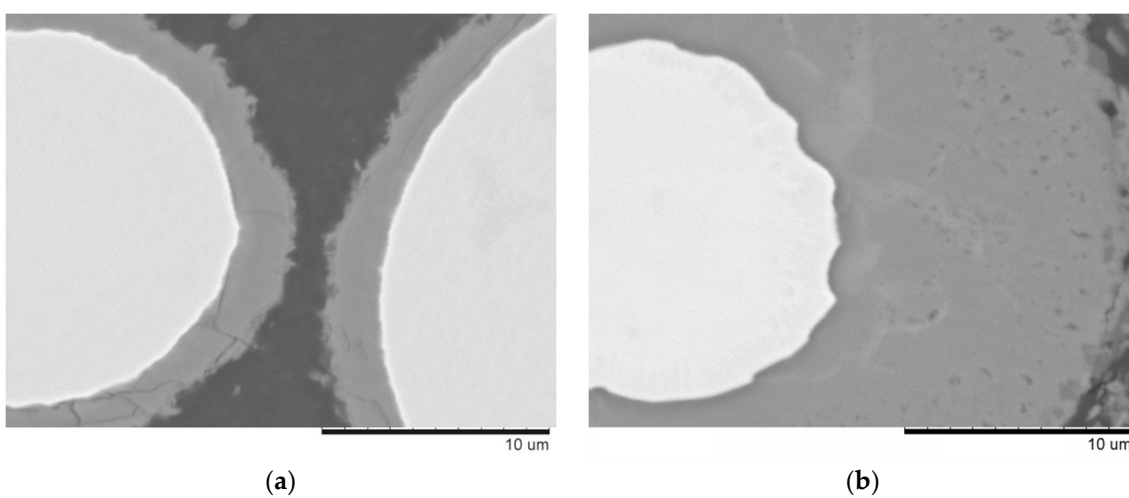


**Figure 4.** Reaction layer formed at the interface: (a) composite sintered at 540 °C, 3 min, (b) composite sintered at 570 °C, 3 min. BSE images.

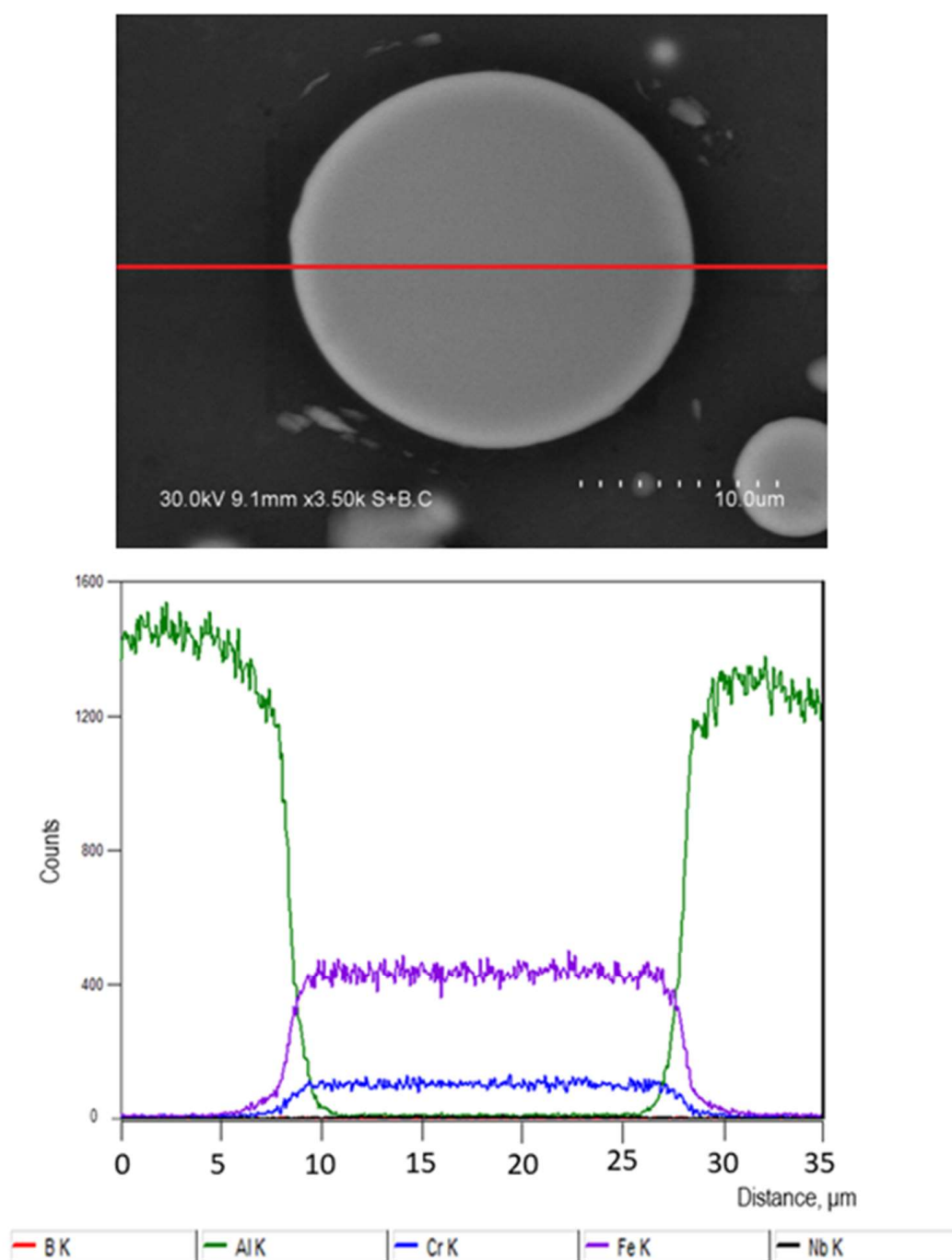


**Figure 5.** Fe-based alloy particle in an Al matrix, composite sintered at 540 °C, no holding, and results of the energy-dispersive spectroscopy (EDS) analysis along the red line on the image.

The compression true stress-true strain curves are presented in Figure 7. The sintered and sintered/forged Al-20 vol.% Fe<sub>66</sub>Cr<sub>10</sub>Nb<sub>5</sub>B<sub>19</sub> composites having no reaction layer and the composite having a thin reaction layer showed similar mechanical behavior and close values of the offset yield strength (110–140 MPa). They were very ductile, allowing for more than 50% true strain in compression (Table 1). The same values of yield strength of the sintered unreinforced aluminum and the Al-20 vol.% Fe<sub>66</sub>Cr<sub>10</sub>Nb<sub>5</sub>B<sub>19</sub> composite obtained at 540 °C without holding (110 MPa) indicate that strengthening is not efficient with these microstructural parameters. After forging, a composite with a higher yield strength (140 MPa) was obtained. This increase in the yield strength can be caused by disruption of continuity of the oxide films present on the particle surfaces upon forging.



During the forging operation, the material experiences both compression and shear. The broken oxide films may act as reinforcing elements ensuring oxide particle contribution to strengthening. The yield strength of the composite having a thin reaction product layer (SPS at 540 °C, 3 min) is 130 MPa, which is higher than that of the composite, in which no reaction layer was detected by SEM (110 MPa). At the same time, the yield strength of the latter is higher than that of the Al-20 vol.%  $\text{Fe}_{74}\text{Mo}_4\text{P}_{10}\text{C}_{7.5}\text{B}_{2.5}\text{Si}_2$  composite (81 MPa) obtained in ref. [7]. This can be due to a finer aluminum powder used in the present work. A finer powder usually contains a higher concentration of oxide, which serves as an additional reinforcement, as noted above.

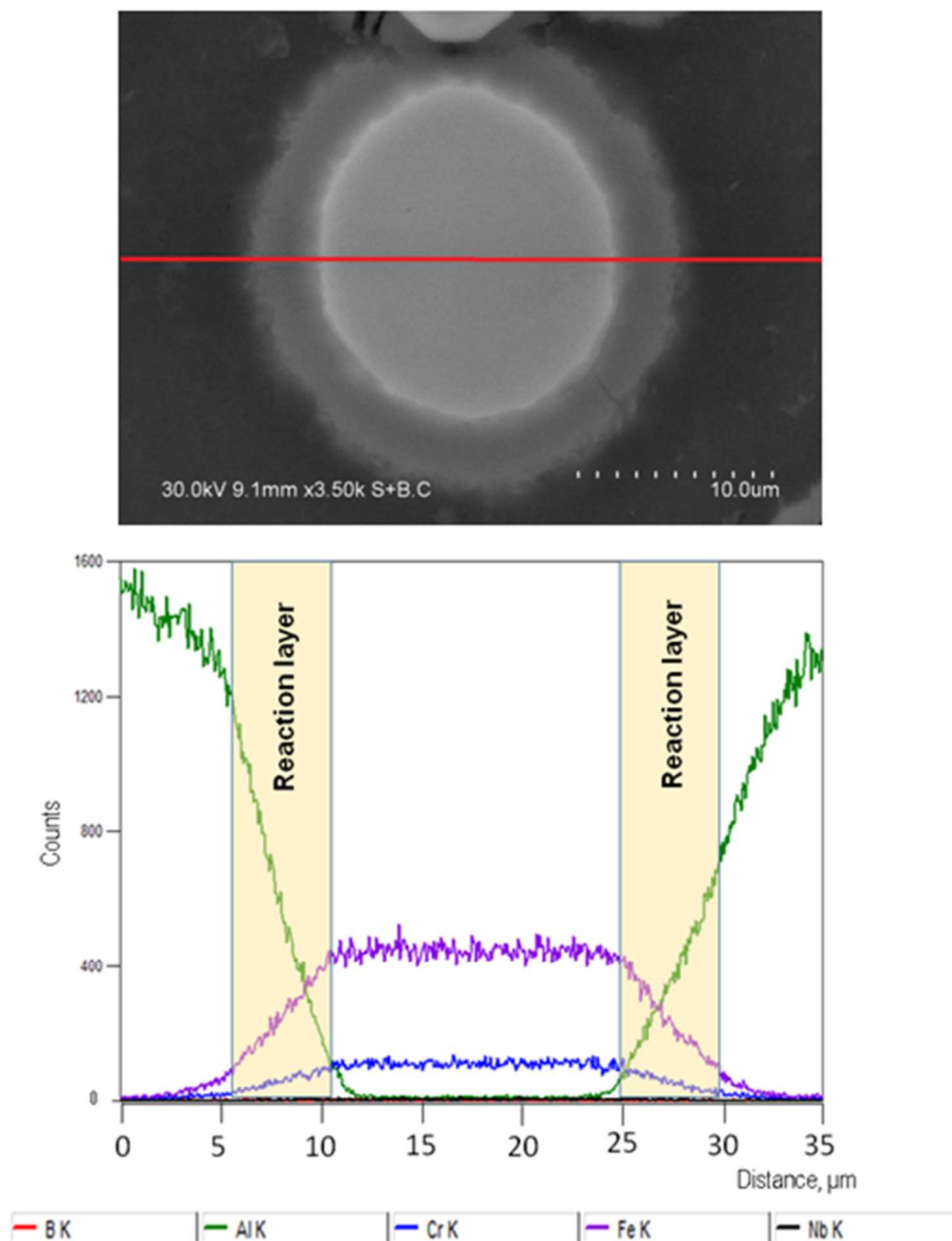


**Figure 6.** Fe-based alloy particle in an Al matrix, composite sintered at 540 °C, 3 min, and results of the EDS analysis along the red line on the image.

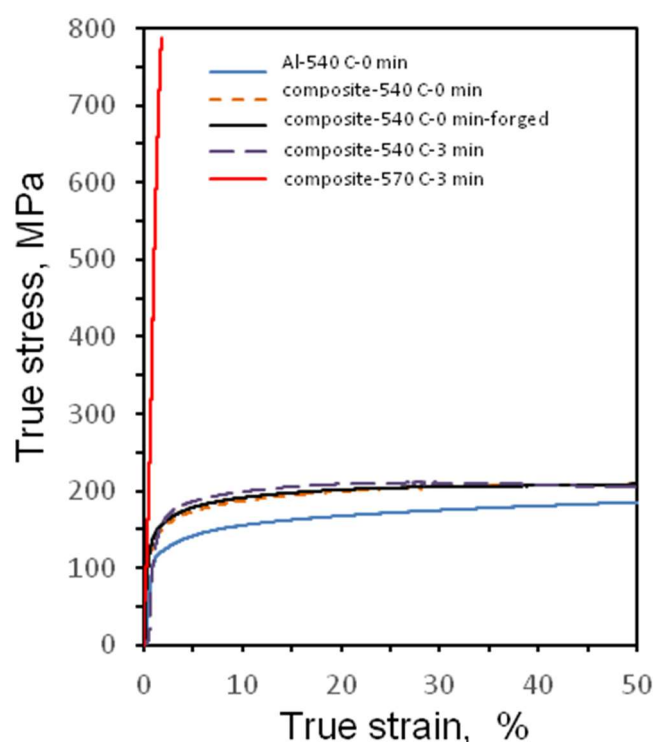


**Figure 7.** Compression true stress-true strain curves of composites obtained from Al-20 vol.%  $\text{Fe}_{66}\text{Cr}_{10}\text{Nb}_5\text{B}_{19}$  mixtures and the unreinforced sintered aluminum.

**Table 1.** Processing conditions, porosity, matrix content, and mechanical properties of composites obtained from the Al- $\text{Fe}_{66}\text{Cr}_{10}\text{Nb}_5\text{B}_{19}$  powder mixture and sintered aluminum. Average values of the offset yield strength and ultimate strength are reported along with standard deviations.

Powder	Processing Conditions of Powders	Porosity, %	Al Matrix Volume Fraction, %	Offset Yield Strength $\sigma_{0.2}$ , MPa	Ultimate Strength, MPa	Strain
Al	SPS, 540 °C, 0 min	<1	100	$110 \pm 5$	-	Plastic strain >50%
Al-20 vol.% $\text{Fe}_{66}\text{Cr}_{10}\text{Nb}_5\text{B}_{19}$	SPS, 540 °C, 0 min	<1	80	$110 \pm 5$	-	Plastic strain >50%
Al-20 vol.% $\text{Fe}_{66}\text{Cr}_{10}\text{Nb}_5\text{B}_{19}$	SPS, 540 °C, 0 min, forging	<1	80	$140 \pm 5$	-	Plastic strain >50%
Al-20 vol.% $\text{Fe}_{66}\text{Cr}_{10}\text{Nb}_5\text{B}_{19}$	SPS, 540 °C, 3 min	<1	67	$130 \pm 5$	-	Plastic strain >50%
Al-20 vol.% $\text{Fe}_{66}\text{Cr}_{10}\text{Nb}_5\text{B}_{19}$	SPS, 570 °C, 3 min	<1	37	-	$780 \pm 10$	Deformation at fracture 2%

The composite sintered at 570 °C for 3 min featured a thick reaction product layer and contained only 37 vol.% of residual aluminum (Table 1). This material showed a high compressive strength (790 MPa) and a fracture strain of 2%. The product of the interaction between aluminum and the metallic glass ( $\text{FeAl}_3$ ) acts as a reinforcing element via a load transfer mechanism, contributing to an increased strength of the composite. The fracture surface of this composite shows areas of the Fe-based alloy particles (bright areas) and reaction product layer (light-gray areas), which fracture in the brittle mode (Figure 8a). Areas of the matrix (dark-gray areas) showed a dimple fracture surface (Figure 8a). A higher magnification image of a Fe-based alloy particle surrounded by a layer of the reaction products is presented in Figure 8b. Noteworthy is the absence of debonding at the

Fe-based alloy particle/reaction product interface. The Fe-based alloy particles were not pulled out of the matrix. Rather, they experienced fracture, which indicates strong bonding at the interface. The cores of the reinforcing particles show fracture surface morphologies that are characteristic to amorphous materials.

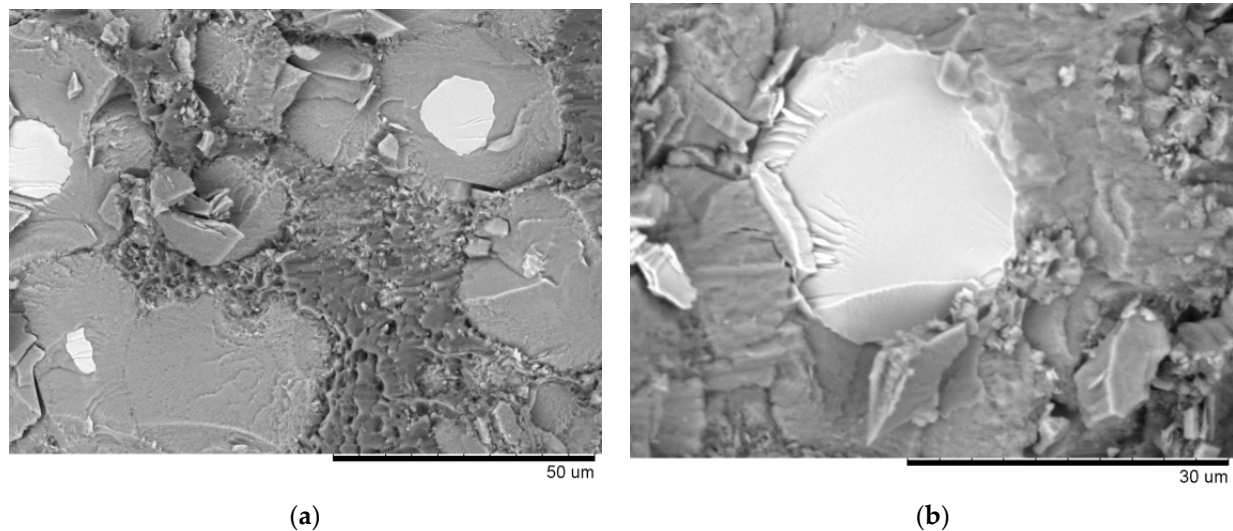


**Figure 8.** Fracture surface of the composite sintered at 570 °C, 3 min, after compression test: (a) an area showing Fe-based alloy particles, reaction products and residual Al matrix, (b) an area showing a Fe-based alloy particle and reaction products. BSE images.

#### 4. Conclusions

The microstructure and mechanical properties of composites obtained by SPS of Al-20 vol.% Fe<sub>66</sub>Cr<sub>10</sub>Nb<sub>5</sub>B<sub>19</sub> mixtures were examined. The sintering conditions were selected such that composites without significant interaction between the matrix and the Fe-based alloy as well as composites with reaction layers of different thicknesses were produced. The SEM/EDS investigations showed that the product layer formed after SPS at 540 °C for 3 min has a gradient structure with Fe/Cr ratio remaining constant across the layer thickness. The sintered and sintered/forged Al-20 vol.% Fe<sub>66</sub>Cr<sub>10</sub>Nb<sub>5</sub>B<sub>19</sub> composites having no reaction layer and the sintered composite having a thin reaction layer showed similar mechanical behavior and close values of yield strength (110–140 MPa). They were very ductile, allowing for more than 50% true strain in compression. The composite sintered at 570 °C for 3 min featured a thick reaction product layer and contained only 37 vol.% of residual aluminum. This material showed a very high compressive strength (780 MPa) and a fracture strain of 2%. The product of the interaction between aluminum and the metallic glass (FeAl<sub>3</sub>) acted as a reinforcing element via a load transfer mechanism, contributing to an increased strength of this composite.

**Author Contributions:** Conceptualization, D.V.D., V.I.K. and K.G.; Methodology, I.S.B., M.A.E. and A.A.M.; Investigation, B.B.B., M.A.L., A.N.N., D.V.D. and V.I.K.; Writing—original draft preparation, V.I.K. and D.V.D.; Writing—review and editing, G.Y.K., B.B.B. and A.V.U.; Supervision, A.G.A. and A.M.J.J.; Project administration, D.V.D.; Funding acquisition, D.V.D. All authors have read and agreed to the published version of the manuscript.

**Funding:** This work was partially funded by the Ministry of Science and Higher Education of the Russian Federation, project 075-15-2020-781.

**Conflicts of Interest:** The authors declare no conflict of interest. The funders had no role in the design of the study; in the collection, analyses, or interpretation of data; in the writing of the manuscript, or in the decision to publish the results.

## References

- Chawla, K.K. *Composite Materials: Science and Engineering*, 2nd ed.; Springer: Berlin/Heidelberg, Germany, 1998; 483p.
- Lee, J.-M.; Kang, S.-B.; Sato, T.; Tezuka, H.; Kamio, A. Microstructures and mechanical properties of Al3Fe reinforced aluminum matrix composites fabricated by a plasma synthesis method. *Mater. Trans.* **2002**, *43*, 2487–2493. [\[CrossRef\]](#)
- Himmler, D.; Randelzhofer, P.; Körner, C. Formation kinetics and phase stability of in-situ Al3Ti particles in aluminium casting alloys with varying Si content. *Results Mater.* **2002**, *7*, 100103. [\[CrossRef\]](#)
- Shadangi, Y.; Sharma, S.; Shivam, V.; Basu, J.; Chattopadhyay, K.; Majumdar, B.; Mukhopadhyay, N.K. Fabrication of Al-Cu-Fe quasicrystal reinforced 6082 aluminium matrix nanocomposites through mechanical milling and spark plasma sintering. *J. Alloys Compd.* **2020**, *828*, 154258. [\[CrossRef\]](#)
- Yuan, Z.; Tian, W.; Li, F.; Fu, Q.; Hu, Y.; Wang, X. Microstructure and properties of high-entropy alloy reinforced aluminum matrix composites by spark plasma sintering. *J. Alloys Compd.* **2019**, *806*, 901–908. [\[CrossRef\]](#)
- Yuan, Z.; Tian, W.; Li, F.; Fu, Q.; Wang, X.; Qian, W.; An, W. Effect of heat treatment on the interface of high-entropy alloy particles reinforced aluminum matrix composites. *J. Alloys Compd.* **2020**, *822*, 153658. [\[CrossRef\]](#)
- Wang, Z.; Scudino, S.; Stoica, M.; Zhang, W.; Eckert, J. Al-based matrix composites reinforced with short Fe-based metallic glassy fiber. *J. Alloys Compd.* **2015**, *651*, 170–175. [\[CrossRef\]](#)
- Kotov, A.D.; Mikhaylovskaya, A.V.; Mochugovskiy, A.G.; Medvedeva, S.V.; Bazlov, A.I. Aluminum alloy matrix composite reinforced with metallic glasses particles using hot-roll bonding. *Rus. J. Non-Ferrous Metals* **2020**, *61*, 297–302. [\[CrossRef\]](#)
- Perrière, L.; Champion, Y. Phases distribution dependent strength in metallic glass–aluminium composites prepared by spark plasma sintering. *Mater. Sci. Eng. A* **2012**, *548*, 112–117. [\[CrossRef\]](#)
- Dudina, D.V.; Georgarakis, K.; Aljerf, M.; Li, Y.; Braccini, M.; Yavari, A.R.; Inoue, A. Cu-based metallic glass particle additions to significantly improve overall compressive properties of an Al alloy. *Compos. Part A* **2010**, *47*, 1551–1557. [\[CrossRef\]](#)
- Aljerf, M.; Georgarakis, K.; Louzguine-Luzgin, D.; Le Moulec, A.; Inoue, A.; Yavari, A.R. Strong and light metal matrix composites with metallic glass particulate reinforcement. *Mater. Sci. Eng. A* **2012**, *532*, 325–330. [\[CrossRef\]](#)
- Wang, Z.; Georgarakis, K.; Nakayama, K.Y.; Li, A.; Tsarkov, G.; Xie, D.; Dudina, D.; Louzguine, A.R. Yavari, Microstructure and mechanical behavior of metallic glass fiber-reinforced Al alloy matrix composites. *Sci. Rep.* **2016**, *6*, 24384. [\[CrossRef\]](#)
- Dudina, D.V.; Bokhonov, B.B.; Batraev, I.S.; Amirastanov, Y.N.; Ukhina, A.V.; Kuchumova, I.D.; Legan, M.A.; Novoselov, A.N.; Gerasimov, K.B.; Bataev, I.A.; et al. Interaction between Fe66Cr10Nb5B19 metallic glass and aluminum during spark plasma sintering. *Mater. Sci. Eng. A* **2021**, *799*, 1–13. [\[CrossRef\]](#)
- Li, Z.; Zhang, M.; Li, N.; Liu, L. Metal frame reinforced bulk metallic glass composites. *Mater. Res. Lett.* **2020**, *8*, 60–67. [\[CrossRef\]](#)
- Zhang, L.; Narayan, R.L.; Fu, H.M.; Ramamurty, U.; Li, W.R.; Li, Y.D.; Zhang, H.F. Tuning the microstructure and metastability of  $\beta$ -Ti for simultaneous enhancement of strength and ductility of Ti-based bulk metallic glass composites. *Acta Mater.* **2019**, *168*, 24–36. [\[CrossRef\]](#)
- Zhang, X.; Chen, T.; Ma, S.; Qin, H.; Ma, J. Overcoming the strength-ductility trade-off of an aluminum matrix composite by novel core-shell structured reinforcing particulates. *Compos. Part B* **2021**, *206*, 108541. [\[CrossRef\]](#)
- Guan, H.D.; Li, C.J.; Gao, P.; Prashanth, K.G.; Tan, J.; Eckert, J.; Tao, J.; Yi, J.H. Aluminum matrix composites reinforced with metallic glass particles with core-shell structure. *Mater. Sci. Eng. A* **2020**, *771*, 138630. [\[CrossRef\]](#)
- Suryanarayana, C.; Inoue, A. Iron-based bulk metallic glasses. *Int. Mater. Rev.* **2013**, *58*, 131–166. [\[CrossRef\]](#)
- Salamon, M.; Mehrer, H. Interdiffusion, Kirkendall effect, and Al self-diffusion in iron–aluminium alloys. *Z. Für Met.* **2005**, *96*, 4–16. [\[CrossRef\]](#)
- Karfoul, M.K.; Tatlock, G.J.; Murray, R.T. The behaviour of iron and aluminium during the diffusion welding of carbon steel to aluminium. *J. Mater. Sci.* **2007**, *42*, 5692–5699. [\[CrossRef\]](#)
- Olevsky, E.A.; Dudina, D.V. *Field-Assisted Sintering: Science and Applications*; Springer International Publishing: Cham, Switzerland, 2018; 425p.
- Kuchumova, I.D.; Batraev, I.S.; Ukhina, A.V.; Borisenko, T.A.; Bulanov, U.E.; Ulianitsky, V.Y.; Dudina, D.V.; Shikalov, V.S.; Kosarev, V.F.; Bataev, I.A.; et al. Processing of Fe-based alloys by detonation spraying and spark plasma sintering. *J. Therm. Spray Tech.* **2021**, *30*, 1692–1702. [\[CrossRef\]](#)
- Yadav, D.; Bauri, R. Development of Cu particles and Cu core-shell particles reinforced Al composite. *Mater. Sci. Technol.* **2015**, *31*, 494–500. [\[CrossRef\]](#)
- Gao, H.; He, Y.; Shen, P.; Zou, J.; Xu, N.; Jiang, Y.; Huang, B.; Liu, C.T. Porous FeAl intermetallics fabricated by elemental powder reactive synthesis. *Intermetallics* **2009**, *17*, 1041–1046. [\[CrossRef\]](#)
- Gao, H.Y.; He, Y.H.; Shen, P.Z.; Jiang, Y.; Liu, C.T. Effect of pressure on pore structure of porous FeAl intermetallics. *Adv. Powder Technol.* **2015**, *26*, 882–886. [\[CrossRef\]](#)